eTransportation 9 (2021) 100130

Contents lists available at ScienceDirect

eTransportation

journal homepage: www.journals.elsevier.com/etransportation

Co-optimization of total running time, timetables, driving strategies and energy management strategies for fuel cell hybrid trains☆

Hujun Peng [a, *], Yuejie Chen [a], Zhu Chen [a], Jianxiang Li [a], Kai Deng [a], Andreas Thul [a], Lars Löwenstein [b], Kay Hameyer [a]

[a] Institute of Electrical Machines (IEM), RWTH Aachen University, Aachen, Germany
[b] Siemens Mobility GmbH, Vienna, Austria

ARTICLE INFO

Article history:
Received 25 March 2021
Received in revised form
23 June 2021
Accepted 13 July 2021
Available online 16 July 2021

Keywords:
Fuel cell trains
Co-optimization
Train control
Train timetabling
Dynamic programming
Energy management

ABSTRACT

A co-optimization of the total running time, timetables, driving strategies and energy management is implemented for the world's first commercial fuel cell train *Coradia iLint* in this contribution. Thereby, the forward dynamic programming algorithm is applied to co-optimize the driving strategies between two stations, the running time distribution in various railway sections and the entire journey's running time. Through parallelization of the algorithm, the computational time is reduced. For energy management, a rule-based strategy utilizing the convexity of the fuel cell system's consumption curve is introduced. The co-optimization of train control and energy management is realized using a sequential algorithm to achieve decoupling. As a result, the number of state variables while using dynamic programming for the co-optimization is maintained at two. Through the co-optimization of the running time, timetables and driving strategies, the optimal running time is determined, which is about 8 min less than the existing time table while consumes 1.8 % less energy. Furthermore, through the co-optimization of the speed profiles and the energy management, evident energy consumption decreases if a short running time is required. Thereby, the hydrogen consumption decreases by 3.8 % after the co-optimization compared to that before co-optimization under the minimal drive time of 4615 s for a total distance of 82.6 km.

1. Introduction

1.1. Background and motivation

About 24 % of direct carbon dioxide emissions from fuel combustion comes from transportation [1]. At a time when global emissions require to decrease, transport carbon dioxide emissions are on the increase [2]. Road vehicles make nearly three-quarters of carbon dioxide emissions in the transport area. Thereby, rail belongs to the most energy-efficient transport forms, which uses 3 % of the total energy to afford 7 % of freight transport and 9 % of passenger mobility [3]. Therefore, the emissions are expected to be reduced by promoting lower emission transport forms like trains and using renewable energy.

Until 2020, around 40 % of the railway network in Germany is served by combustion engines-driven trains. The target of German federal government is to reach 70 % electrification of the railway network by 2025 [4]. Nevertheless, it is not economically profitable to electrify routes with low train frequency because of the required vast capital investment and the significant amount of infrastructure. Thus, the fuel cell hybrid railway vehicle is a promising medium-term alternative to the combustion-engine driven trains and has begun its commercial operation in multiple countries. In 2018, the world's first commercial fuel cell passenger train started service in Germany [5]. In 2017, *CRRC Tangshan* uncovered the first commercial hydrogen-powered tram globally and finished its first experiment run in China [6]. In America, the first hydrogen-powered train was reserved for operation in California in November 2019 [7].

The hydrogen-powered hybrid trains are equipped with two energy sources: fuel cells as high-capacity active controllable power sources and high voltage batteries as a high-power

☆ This research is supported by the German Federal Ministry of Transport and Digital Infrastructure (BMVi), with the funding numbers of 03B10502B and 03B10502B2.

* Corresponding author.
E-mail address: hujun.peng@iem.rwth-aachen.de (H. Peng).

https://doi.org/10.1016/j.etran.2021.100130
2590-1168/

rechargeable energy storage system. Due to high voltage battery, kinetic energy can be largely recycled into batteries rather than grids during regenerative braking. Compared to the fuel cell hybrid trains, the combustion-engine driven trains do not recycle kinetic energy. For the electrical trains supplied by overline catenaries, they can not store electrical energy onboard and recycle the mechanical energy to use for other trains in the acceleration phase at the same time. As learned from literature, a co-optimization of timetables and train driving strategies in each section of the whole journey should be carried out to minimize the total energy consumption [8]. No literature has been found to handle the optimization problem of timetables and driving strategies for fuel cell hybrid trains since the fuel cell hybrid train came to commercial service in 2018. Furthermore, in the literature related to traditional railway operation, the whole journey's total running time is fixed before the co-optimization. However, the presumed fixed running time is not optimized, especially when the ancillary consumption, which makes a large portion of the total consumption, is almost linear to the running time. Therefore, the total running time should also be optimized to reduce the total energy consumption. Besides that, due to the hybrid configuration of the fuel cell hybrid trains, energy management, which distributes load power between fuel cell systems and battery systems, should also be considered because energy management directly determines fuel cells' working points or hydrogen consumption. Therefore, for the fuel cell hybrid trains, energy consumption can be reduced through a co-optimization of the total running time, timetables, driving strategies and energy management, which researchers have not studied thus far.

1.2. Literature review

Both train timetabling and control influence energy consumption. Therefore, in the following, the literature study about train operation contains two parts including the energy-efficient train control and the energy-efficient train timetabling. A detailed review paper can be found in Refs. [9,10]. After introducing train operation, a brief outline of the most advantageous energy management strategies for hydrogen-powered hybrid vehicles will be given.

1.2.1. Energy-efficient train operation

The energy-efficient train control is understood as optimizing the speed profile between two stations to reduce energy consumption under a fixed running time. Various methods or algorithms are utilized to solve the energy-efficient train control problem, including Pontryagin's Maximum Principle (PMP), pseudospectral methods, heuristic algorithms and dynamic programming. Mathematically, the energy-efficient train control belongs to the optimal control problem, which suffers from various state and control constraints such as maximum speed limits and traction power limits. So far, PMP application in energy-efficient train control has been comprehensively studied [10]. According to the PMP theory, the optimal energy-efficient train control for a flat track without considering regenerative braking contains four driving regimes including maximum traction, coasting, cruising and maximum braking [11]. For the electrical trains supplied by the grid, regenerative braking is available. Therefore, the optimal control of the train running on a flat track under the constant speed constraint includes seven driving patterns. They are the maximum traction, cruising with part traction, cruising with part regenerative braking, cruising with full regenerative braking and partial mechanical braking, coasting, full regenerative braking, full regenerative braking plus mechanical braking [12]. Using the PMP conclusions, the optimal control problem is simplified to find the optimal order of the driving patterns mentioned above and determine the shift point from one pattern to another [10]. The uniqueness of the optimal control solution is also proved in Ref. [13]. However, in the real application, varying speed limits and gradients should be considered. For the piecewise constant speed limits and gradients, in Ref. [14], the total distance between two stations is divided into segments of the same constant gradients and speed limits. Then, in each segment, the gradient and speed limit remains constant, and the conclusions of the optimal control consisting of certain driving regimes can be used. Thereby, an algorithm consisting of two loops with the outer loops searching the cruising speed for each section and the inner loop to determine the optimal switching points within each section is developed. In Ref. [15], the track is divided into subsections with constant gradient and speed limits, and in each subsection, an operation sequence of maximum traction, cruising, coasting and maximum braking is assumed. In order to make the calculation more convenient, the constraints related to engines are simplified to have a piecewise affine function or constant value. Each driving regime's duration in each subsection is to be searched using nonlinear programming. In the steep gradient case, in Ref. [16], it is proved that the accelerating phase and the coasting phase interrupt the cruising phase for upcoming steep uphill and downhill parts, separately. It is worth mentioning that the PMP-based algorithm is computationally efficient and it can be used for real-time application.

If the gradient varies continuously or the number of gradient values is too large, the methods based on PMP conclusions can not handle the optimal control problem efficiently. Therefore, the pseudospectral method is utilized to convert the original optimal control problem into a nonlinear programming problem using discretization on the first-order differential equations in the optimal control, which corresponding solvers can solve [17]. The detailed introduction of using the pseudospectral method to determine the optimal train control is described in Ref. [18]. Through the pseudospectral method, various complicated limits related to machines, gradients, speed limits and arrival time window constraints in certain stations can be handled. In Ref. [19], the optimal train control under consideration of regenerative braking, whose maximal force is a nonlinear function of the speed, is implemented using the pseudospectral method. Thereby, in comparison to pure mechanical braking, combined mechanical and electrical braking results in higher fuel efficiency. In Ref. [18], the target time window constraint at each station is considered to investigate how much energy can be saved if a time window instead of a specific time point at each stop is required. However, there is a compromise between the computational time and the solution quality using the pseudospectral method, whereby the discretization degree plays a crucial role. Generally, the pseudospectral method is an offline algorithm. In Ref. [17], PMP is used to confirm and advance the pseudospectral method's results to derive the optimal train control strategy. If the constraints and the resistance force can be linearized, the algorithm of mixed-integer linear programming can be used, which can be applied online due to its high computational efficiencies [20,21]. However, this assumption is not the case in reality.

For the heuristic algorithm, sub-optimal solutions are expected. Certain patterns, including various parameters to be optimized, are used to drive the train. Various evolutionary algorithms can find these parameters. In Ref. [22], the whole distance is divided into segments with constant gradient and speed limits. Four driving regimes containing maximal acceleration, cruising, coasting and maximal braking are assumed within each segment. An evolutionary algorithm is used to search the corresponding running time of different driving regimes within each segment. In Ref. [23], the

velocity values at preset positions are optimized to minimize energy consumption, which can be used as a driver assisting system. The ant colony optimization as well as genetic algorithm are used separately to optimize the speed profile between two stations. As a comparison, offline dynamic programming is used. Dynamic programming performs best, while genetic algorithm and ant colony optimization do not outperform each other dominantly. Since the heuristic algorithm can not determine the optimal solution, its study does not lie in the research field's central focus.

Besides the PMP algorithm, for the optimal solution of the energy-efficient train control, dynamic programming can also solve the optimal control problem. One of the greatest advantages of dynamic programming compared to PMP lies in the fact that all complicated constraints related to machines, timetables, gradients and speed limits can be handled easily [24]. In Ref. [25], dynamic programming and optimal control theory are reviewed, which optimize running profiles between two stations and control battery charging simultaneously to reduce electricity consumption for a train with onboard batteries. Thereby, a backward dynamic programming algorithm is used, the same as found in almost all literature related to optimizing speed profiles by using dynamic programming. However, the terminal boundary condition at the end station is problematic to handle. Thereby, there are errors in the velocity and driven distance at the end station. In order to improve the computational efficiency, in Ref. [26], a novel dynamic programming algorithm based on an event-based discretization instead of an even discretization in the time and space domain is implemented to determine the optimal velocity profile between two stations. The search space is reduced so that an online implementation of the algorithm is possible. So far, the dynamic programming algorithm has been comprehensively studied by various researchers to optimize the speed profile of trains driven by combustion-engines or pure electrical motors. However, the fuel cell hybrid train, whose control optimization requires a co-optimization of energy management and driving strategies, has not been studied using dynamic programming. More importantly, as mentioned before, integration of the total running time optimization is also desired. Since backward dynamic programming is used, the optimal driving profile corresponding to different running time values requires multiple dynamic programming runs, which is not time efficient. Furthermore, it is worth mentioning that dynamic programming requires a computational load enormously larger than PMP [27]. Therefore, dynamic programming is not the research focus to optimize the driving strategies between two stations, as it is not online implementable now and limited by the existing computational resources. However, as communication and computation technology develops, it is possible to execute the computation outside the train.

Besides the energy-efficient train control between two stations, the optimization of train timetables plays another important role in reducing the whole journey's energy consumption. The optimization of timetables contains two aspects: distribution of running time for the single-train operations and synchronization of acceleration and regenerative braking for the multiple-train operation [8]. As the fuel cell hybrid trains have their own large batteries and no overlines exist, the synchronization problem is not faced and will not be discussed in the paper. For the running time distribution of a single train operation, in Ref. [28], dynamic programming is used to reschedule the high-speed railway traffic to reduce the total delay time. In Ref. [29], by modifying train running times in different sections for regional trains with backward dynamic programming, the chance of getting connections to other public buses at metro stations is increased. It is worth mentioning that the timetables or the distribution of the total running time in each railway section determine the realizable minimum of energy consumption. Therefore, a co-optimization of timetables and driving strategies is required and lies in the research focus [30]. In Ref. [31], a two-level optimization algorithm is used to co-optimize the timetables and the driving strategies. The evolutionary algorithm is used to distribute the total fixed journey time in different sections on the first level. On the second level, the PMP-based algorithm, as described before, is used to optimize the driving strategies between two stations for the assigned running time. In Ref. [32], the first level uses the simulated annealing algorithm, and the second level uses dynamic programming to determine the energy-efficient train control under the assigned running time. Besides the algorithms based on evolutionary algorithms, the pseudospectral method, which was introduced before, can optimize the timetable and the driving cycles simultaneously. In Ref. [33], the timetable with a given fixed total running time is optimized under consideration of flexible departure and arrival time window constraints at each substation in between. The problem is rewritten into multi-phase optimal control and resolved using the pseudospectral method, which considers conditions of varying gradients and speed limits. In Ref. [34], the method based on PMP and the pseudospectral algorithms are introduced and compared to optimize traveling time supplements for a journey with various stops and a fixed total running time. Thereby, piecewise gradient and velocity limits are considered.

1.2.2. Energy management

Besides timetable and driving strategies optimization, the power distribution for the hydrogen-powered hybrid railway vehicles strongly influences the fuel economy. Two kinds of energy management strategies are often found in literature reviews about hybrid vehicles, namely optimization-based and rule-based power distribution methods [35]. In Ref. [36], various power distribution strategies are studied for hybrid systems consisting of battery and capacitor considering battery aging and energy efficiency. In Ref. [37], the power distribution strategies are analyzed for fuel cell hybrid vehicles assisted with ultracapacitors, which however does not include optimization-based strategies. In Ref. [38], the Markov prediction method is adopted to realize velocity prediction for a short period and the optimal power distribution under the prediction will be calculated by using dynamic programming. However, coupling between energy management and the optimizing driving cycle is not mentioned. Summarily, the most desired characteristics of energy management strategies include optimality, healthy operation, adaptivity, causality and scalability. The optimality refers to the fuel economy, which should maintain the fuel cell systems operating efficiently for fuel cell railway vehicles. Under healthy operation, the fuel cell systems should work stable without high dynamic power change. Adaptivity is required for online strategies in real-time applications. The causality assumes that less future information is required for the implementation of online strategies. The most challenging point, namely the scalability, describes that the online strategies developed for one application can be transferred to other areas without difficulties. Few papers about online strategies for hybrid vehicles include all the mentioned characteristics. Last year, we developed model-based strategies to solve the challenges mentioned above, including a rule-based strategy and an adaptive Pontryagin's Minimum Principle-based strategy (APMP). In Ref. [39], the rule-based strategy, which utilizes the convexity of fuel cells' consumption curve, is introduced. Compared to offline reference strategies, a good fuel economy and a healthy fuel cell system's operation are realized. In Ref. [40], a physical formula is derived to estimate the costate defined in the optimal control. Thereby, a scalable and casual APMP strategy is introduced, which has an extremely near-optimal fuel economy compared to offline results. In Refs. [41,42],

the rule-based and the APMP-based strategies are validated by using test bench measurement, respectively. Since the fuel cell power under the APMP strategy is more dynamic than the rule-based strategy, which shortens fuel cells' lifetime. Therefore, the rule-based strategy is applied in the co-optimization in this contribution.

1.2.3. Motivation

Overall, the co-optimization of running time, timetables, driving strategies and energy management, which the fuel cell hybrid trains face, has not been studied. Furthermore, various complicated constraints related to traction and regenerative braking, whose maximal force is nonlinear to motor speed and time window at each station, under consideration of continuous varying speed limits and gradients, should be considered.

1.3. Main work

Due to the complexity of the problem, the forward dynamic programming is used to co-optimize the total running time, timetables and driving strategies. Then, an adaptive rule-based strategy is used for the power distribution strategy due to its high adaptivity, scalability and fuel efficiency. The major contributions are summarized in the following:

- Two-layer dynamic programming is adopted to co-optimize driving strategies between stops, timetables and the total running time to reduce energy consumption. The first layer of dynamic programming is two-dimensional, which uses velocity, and distance as the state variables, time as the independent variable. Thereby, it optimizes driving strategies between every two nearby stops under various driving times. The second layer of dynamic programming is one-dimensional and helps minimize energy consumption by adjusting timetables and the total running time.
- The co-optimization of driving strategies, timetables, and the total running time is further developed considering the online rule-based power distribution method for the hydrogen-powered hybrid trains.

1.4. Outline of the paper

In section 2, the train modeling is introduced. In section 3, the two-dimensional forward dynamic programming is adopted to solve the optimal train control and timetable problem. In section 4, a quantitative formula that utilizes the convexity of the fuel cell system's consumption curve is derived to define the rule, and the rule-based strategy is introduced. In section 5, the co-optimization between the speed profile and the rule-based strategy is introduced, with their mutual influence on each other considered. In section 6, the conclusions and outlooks will be summarized.

2. Power train modeling

Fig. 1 shows the configuration of the power train that simulates the power flow of a half train. The fuel cell system and the battery are connected parallel to the DC bus. In this work, only the train velocity and the battery SoC are dynamically calculated. For other components, lookup tables are applied to model their power losses. In Ref. [40], the modelling of each part in the driveline is described in detail.

2.1. Environment model

As a driving cycle, the train speed trajectory between Bremervörde and Cuxhaven with 14 stations and a total distance of 82.6 km is generated. It is a part of Alstom Coradia iLint1, which is the route of the world's first passenger train powered by hydrogen fuel cell. The time table of this route is listed in Table 1. The corresponding slope and elevation information are shown in Fig. 2.

2.2. Longitudinal dynamic

The longitudinal dynamics of the train are shown in Fig. 3 and can be described as:

$$F_{\mathrm{a}} = F_{\mathrm{trac}} - F_{\mathrm{roll}} - F_{\mathrm{aero}} - F_{\mathrm{grade}} - F_{\mathrm{b}}, \tag{1}$$

where F_{a} is the acceleration force, F_{trac} the traction force, F_{roll} the rolling resistance, F_{grade} the uphill resistance, F_{aero} the aerodynamic drag and F_{b} the mechanical braking force. It can be rewritten as follows:

$$m\frac{\mathrm{d}v}{\mathrm{d}t} = F_{\mathrm{trac}} - c_{\mathrm{roll}}mg\cos(\varphi) - 0.5\rho C_{\mathrm{d}}A_{\mathrm{f}}v^2 - mg\sin(\varphi) - F_{\mathrm{b}}, \tag{2}$$

where m and v are the equivalent mass and velocity of the train, c_{roll} is the rolling resistance coefficient, φ describes the road slope angle, g refers to the earth gravitational acceleration, ρ to the air density, C_{d} to the drag coefficient and A_{f} to the frontal area of the train. The efficiency of the DC/DC converter and the DC/AC inverter are assumed to be constant values, which are 0.98 and 0.94, respectively. The values of these parameters of a half train are listed in Table 2.

2.3. Electrical machine

Three high-speed asynchronous machines, which are modeled with lookup tables to calculate the machine power losses, support the train traction. The lookup table of power loss in the machines is presented together with the efficiency map in Fig. 4. All parameters corresponding to the electrical machines and the gear system are summarized in Table 3.

2.4. Fuel cell

The rated power of the used Proton Exchange Membrane (PEM) fuel cell system is 200 kW. The entire system has its own controller to adjust its output power. This paper focuses on the co-optimization of train control, timetabling, and energy management to reduce hydrogen consumption rather than the effects of control on fuel cells' aging. Therefore, the characteristic consumption curve is adopted to model fuel cell systems. Fig. 5a shows the experimental measurement of the consumption curve. The approximated curve and its convexity are displayed in Fig. 5b.

The mathematical expression of the convexity of the consumption curve is described as follows:

$$\begin{aligned}\dot{m}_{\mathrm{H_2}}(\alpha \cdot P_{\mathrm{fc},1} + (1-\alpha)\cdot P_{\mathrm{fc},2}) < \alpha \cdot \dot{m}_{\mathrm{H_2}}(P_{\mathrm{fc},1}) \\ + (1-\alpha)\cdot \dot{m}_{\mathrm{H_2}}(P_{\mathrm{fc},2}),\end{aligned} \tag{3}$$

where $\dot{m}_{\mathrm{H_2}}$ stands for the mass flow that is dependent on the fuel cell output power.

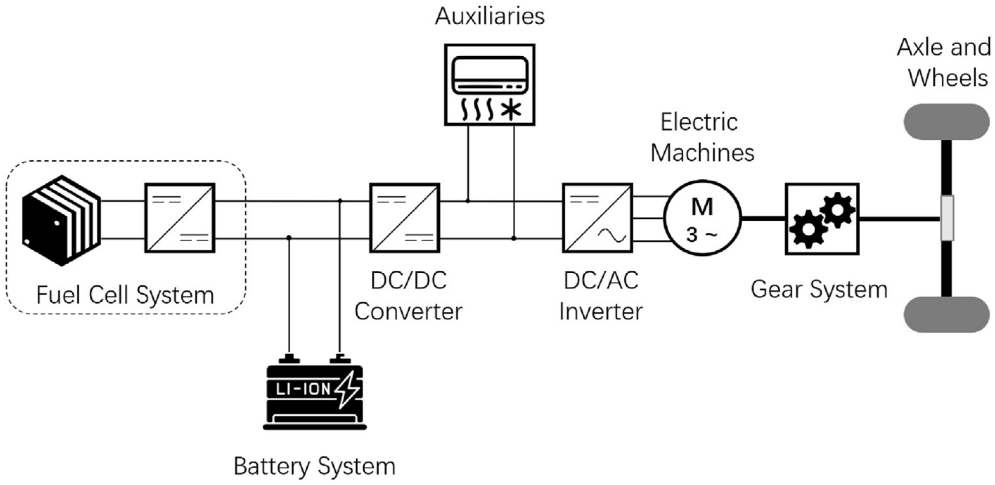

Fig. 1. Configuration of the driveline.

Table 1
Time table of the driving cycle.

Arrival station	Latest arrival time	Stop time	Departure time
Bremervörde	–	–	0 s
Oerel	420 s	30 s	450 s
Heinschenwalde	660 s	60 s	720 s
Frelsdorf	960 s	30 s	990 s
Geestenseth	1200 s	60 s	1260 s
Wehdel	1440 s	60 s	1500 s
Sellstedt	1800 s	60 s	1860 s
Bremerhaven-Wulsdorf	2280 s	30 s	2310 s
Bremerhaven-Hbf	2520 s	960 s	3480 s
Bremerhaven-Lehe	3720 s	60 s	3780 s
Wremen	4440 s	30 s	4470 s
Dorum(Weserm)	4800 s	300 s	5100 s
Nordholz	5700 s	60 s	5760 s
Cuxhaven	6540 s	–	–

2.5. Lithium-ion battery system

The model of the lithium-ion battery cell is parameterized based on measurement data. The battery system has a nominal capacity of 207 Ah and a nominal voltage of 850 V. The battery pack's temperature is assumed to be controlled near 25 °C, and thermal modeling is not taken into account. The technical specifications of the battery are listed in Table 4. The dependence of the battery internal resistance R_0 and the open-circuit voltage on the state of charge is presented in Fig. 6.

3. Co-optimization of running time, timetables, and driving strategies without considering energy management

In this section, the train speed trajectory optimization is formulated as an optimal control problem and the speed profile is generated through two-dimensional dynamic programming with forward iteration.

3.1. Generation of optimal speed profiles dependent on variable running time between two stops

Under the two-dimensional framework, the speed and the position of the fuel cell hybrid railway vehicle are chosen to be the state variables:

$$\boldsymbol{x} = [x_1, x_2] = [v, s]. \tag{4}$$

The discretization of the state variables are changeable and defined unevenly. At the beginning of a section between two stations, the discretization degree of position is 0.1 m. It is gradually increased to 2 m after 40 m. Similarly, the discretization degree is reduced from 2 m to 0.1 m in the last 40 m of the railway section. The reason for the uneven discretization is that the train drives with a relatively low speed when it leaves from or arrives at a station. A higher discretization degree at the beginning and the end ensures a precise calculation and a lower degree in between reduces the computational effort. Generally, the discretization degree of velocity is set to be 0.05 m/s. If the section is longer than 10 km, the

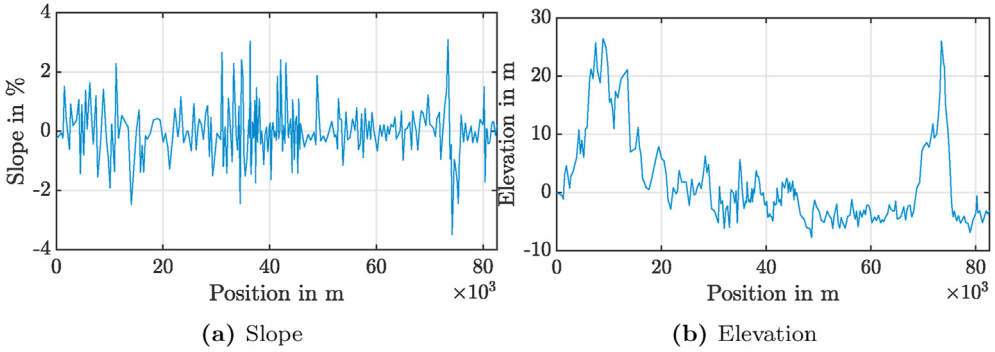

(a) Slope (b) Elevation

Fig. 2. Slope and elevation information of the railway route from Bremervörde to Cuxhaven.

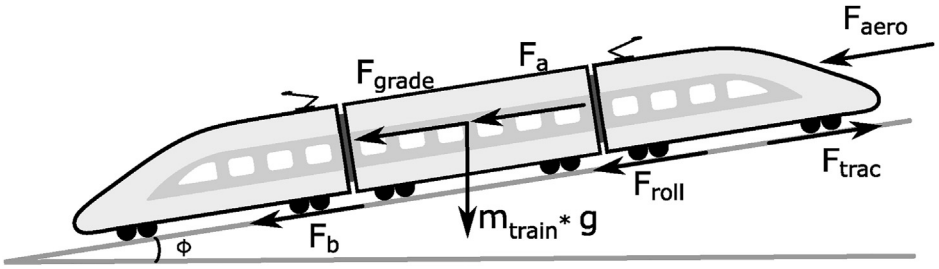

Fig. 3. Longitudinal dynamics of the train.

Table 2
The longitudinal dynamics parameters and environmental conditions.

Parameters	Values
m_{train}	60000 kg (with passengers included)
c_{roll}	0.0015
g	9.81 m/s^2
ρ	1.4 kg/m^3
C_{d}	0.15
A_{f}	10 m^2
$\eta_{\text{DC/DC}}$	0.98
$\eta_{\text{DC/AC}}$	0.94

Table 3
Parameters of the electrical machines and the gear system.

Parameters	Values
number of electrical motors	3
rated power of each machine	220 kW
rated rotational speed	3200 rpm
maximal torque	901 Nm
gear efficiency	0.98
gear ratio	10
wheel radius	0.425 m

discretization degree is changed to 0.1 m/s to reduce the computational demands. The traction or break torque is defined as the control variable:

$$u = M_{\text{el}}. \tag{5}$$

The discretization degree of the torque is 5 Nm. The drive time is discretized with 1 s as the discretization degree. Then, the state equation of the velocity according to the forward dynamic programming is:

$$x_1[k-1] = x_1[k] - a[k], \tag{6}$$

where $a[k]$ is the acceleration, which is calculated based on the longitudinal dynamic, as explained in section 2.2. The dynamic of the position is calculated as follows:

$$x_2[k-1] = x_2[k] - \Delta t \cdot \frac{x_1[k] + x_1[k-1]}{2}. \tag{7}$$

Based on a given railway route, the boundary conditions are defined:

$$x_1[0] = 0, \quad x_1[N] = 0, \quad x_2[0] = 0, \quad x_2[N] = s_{\text{end}} - s_{\text{start}}, \tag{8}$$

where $s_{\text{end}} - s_{\text{start}}$ is the distance between the two adjacent railway stations and the index of the final time stage N.

As the speed limit along the railway section is not to be exceeded and the railway route is given, the state constraints are determined:

$$\begin{aligned} 0 \leqslant & x_1[k] \leqslant v_{\max}(x_2[k]), \\ s_{\text{start}} \leqslant & x_2[k] \leqslant s_{\text{end}}, \end{aligned} \tag{9}$$

where $v_{\max}$ is the speed limit dependent on the position.

The torque of the electric machines has upper and lower limits. When the train accelerates, the required traction force is provided by the electric machines as motors. While the train decelerates, the electric machines work as generators to provide regenerative braking. Besides, if a strong deceleration is required, a mechanical braking can provide additional braking force. Therefore, the control constraint is determined:

$$M_{\text{el, min}}(x_1[k]) - M_{\text{brake, max}} \leqslant u[k] \leqslant M_{\text{el, max}}(x_1[k]), \tag{10}$$

where $M_{\text{el, min}}$ and $M_{\text{el, max}}$ are the minimal and maximal torque of electric machines, which are dependent on motor speed, and $M_{\text{brake, max}}$ the maximal mechanical brake torque. It is worth

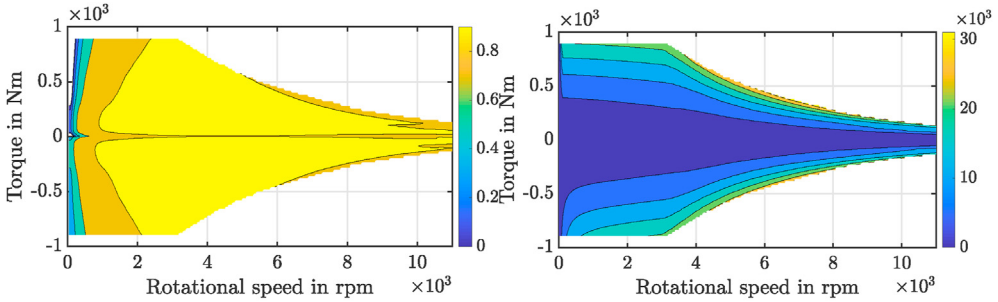

(a) Efficiency (b) P_{loss} in W

Fig. 4. Features of the electrical machine.

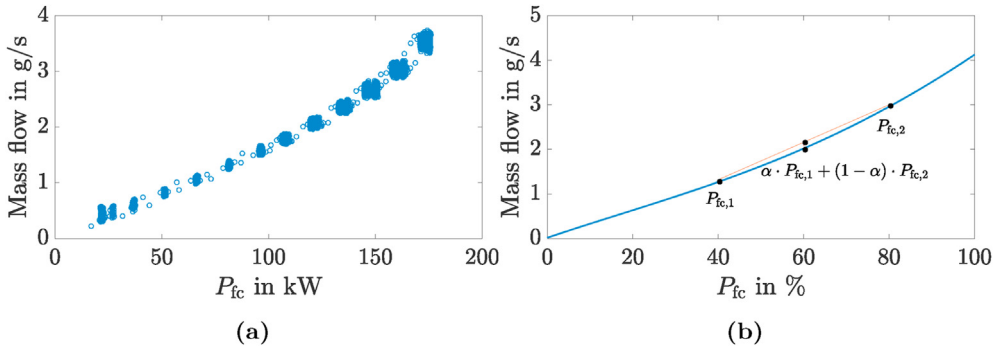

Fig. 5. Characteristic consumption curves of the fuel cell system and its convexity: (a) Experimental measurement, (b) Approximated curve.

Table 4
Parameters of the battery system.

Terms	Values
Rated voltage	835 V
Rated capacity	207 Ah
Number of cells in series	370
Advised SoC range	0.15 ~0.95

mentioning that mechanical braking is utilized only when the required deceleration surpasses the regenerative braking capacity.

The cost function is defined as follows:

$$J = \underbrace{h(x_1[0], x_2[0])}_{\text{initialization}} + \underbrace{\Delta t \cdot \sum_{k=1}^{N} P(x_1[k], u[k])}_{\text{energy consumption}}, \tag{11}$$

where $h(x_1[0], x_2[0])$ represents the initialization based on the speed and position of the train, and $\Delta t \cdot P(x_1[k], u[k])$ is the energy cost in each time interval, which can be presented as a function of speed and torque. The total energy consumption equals the integration of power along the time.

The states dependent cost of the first time stage is initialized at the beginning. In this case, the train starts with a speed of zero from the starting station with a position of zero: $x_1[0] = 0$, $x_2[0] = 0$. Thus, for all other initial states which are greater than zero, an invalid value is assigned to the corresponding cost so that the trajectories, beginning with these states, will not be selected. The initial cost at the first time stage is defined as follows:

$$h(x_1[0], x_2[0]) = \begin{cases} 0 & x_1[0] \leqslant 0,\ x_2[0] \leqslant 0, \\ \infty & \text{otherwise}. \end{cases} \tag{12}$$

The resulting optimal velocity profiles corresponding to various driving times between two stops always begin with zero speed at the start position by using the initialization. As forwarding dynamic programming is used, the boundary condition at the endpoint of railway sections is automatically satisfied without velocity and distance errors.

The transition cost in Eq. (11) can be rewritten and expanded like the following:

$$\begin{aligned} \Delta t \cdot P(x_1[k], u[k]) &= \frac{\Delta t \cdot \omega_{em}(x_1[k]) \cdot u[k]}{1000 \cdot \eta_{D/A} \cdot \eta_{D/D}} \\ &+ \frac{\Delta t \cdot P_{loss}(x_1[k], u[k])}{\eta_{D/A} \cdot \eta_{D/D}} + \frac{\Delta t \cdot P_{aux}}{\eta_{D/D}}, \end{aligned} \tag{13}$$

where $\omega_{em}(x_1[k])$ is the angular velocity of the electric machine in rad/s, $\eta_{D/A}$ is the efficiency of the DC/AC inverter, $\eta_{D/D}$ describes the efficiency of the DC/DC converter, $P_{loss}(x_1[k], u[k])$ is the power loss of the electric machine and P_{aux} indicates the auxiliary power. The values of $\eta_{D/A}$ and $\eta_{D/D}$ are chosen as 0.94 and 0.98, respectively. The auxiliary power is modeled stationary with 45 kW. The angular velocity is calculated as follows:

$$\omega_{em}(x_1[k]) = \frac{x_1[k] \cdot G}{R_{wheels}}, \tag{14}$$

where G is the gear ratio between the axis of electric machines and the wheels, and R_{wheels} describes the radius of wheels.

The optimal control sequence that tries to minimize the total energy consumption along the railway section between two stations is calculated by a forward iteration as follows:

- The states dependent cost of the first time stage is initialized with Eq. (12).

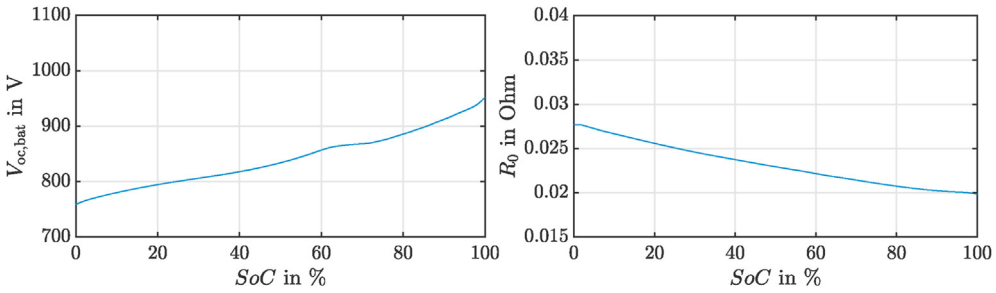

Fig. 6. Features of the battery.

- In the iterative calculation for $k = 1$ to N, at each time stage k: The states of the previous stage $x_1[k-1]$ and $x_2[k-1]$ are calculated with Eq. (6) and Eq. (7), respectively. The cost-to-go matrix of time stage $k-1$ is determined with interpolation and the transition cost matrix is calculated with Eq. (13). By summing up both matrices, the cost-to-go matrix of time stage k is obtained.
- The optimal control variable of time stage k is determined.
- After the iteration to stage N is finished, the optimal control sequence is generated by using a trace-back method.

In this algorithm, a two-dimensional cost-to-go matrix at each time stage k saves the total energy consumption corresponding to all states at that time. In the matrix, each row corresponds to a train speed and each column corresponds to a train position. The element at position $[x_1 = 0, x_2 = s_{\text{end}} - s_{\text{start}}]$ represents the total energy consumption when the train stops at its destination. If a value exists in this element of the cost-to-go matrix for a given time stage k, it indicates that the train is able to reach its destination at time k. Then, this cost-to-go value describes the total energy consumption of the hydrogen-powered train to reach its destination at this time stage. Thus, through the forward dynamic programming, the minimal energy consumption corresponding to the different drive time between two stations is determined, as well as the corresponding optimal control sequence corresponding to different drive time.

3.2. Results

For the given driving cycle, the speed profile between each two stations is analyzed. Fig. 7 shows the energy consumption corresponding to different drive time of several sections as examples.

The points of minimal and maximal drive time are marked with red circles. The speed profile with the minimal energy consumption refers to the lowest point of the curve, highlighted with a red cross. It is observed that the longest drive time might not minimize the energy consumption. Thus, it is crucial to choose an optimal drive time for each section. The shortest, optimal and longest drive time and their corresponding energy consumption of all driving sections are listed in Table 5.

As the speed profile of each section with the optimal drive time is generated, it can be integrated to determine the driven distance. By comparing the calculated distance and the real distance, a deviation can be observed, as listed in Table 6. Due to the high discretization degree, the difference in distance is extremely small and can be neglected. Additionally, the calculation time and utilized memory can be found in Table 6, too. Besides, in the generated speed profiles, the initial and final speed always equals zero, this is realized by the tricky initialization of the cost function and the backward trace back.

3.3. Co-optimization of the total running time, the timetable and the driving strategies

In the previous part, the optimal speed profile between two stops is determined corresponding to different admissible drive time. Notably, the drive time distribution among different railway sections also influences the energy consumption for the entire driving cycle. Therefore, the energy consumption can be decreased further by optimizing the drive time distribution.

Thus, the optimization of drive time distribution is formulated as an optimal control problem. Here, one-dimensional dynamic programming is adopted. The discretized stages are the stops on the route.

The state variable is the arrival time at each station:

$$x[k] = T_{\text{arrival}}[k], \tag{15}$$

where $T_{\text{arrival}}[k]$ is the arrival time at the k-th stop.

The control variable is the drive time between two adjacent stations:

$$u[k] = T_{\text{drive}}[k], \tag{16}$$

where $T_{\text{drive}}[k]$ is the drive time between the k-th station and the previous station.

The dynamic of states indicates that the arrival time at the previous station $k-1$ is related to the arrival time at the current station and the drive time from the previous station to current station.

$$x[k-1] = x[k] - u[k]. \tag{17}$$

The state variable shall not exceed the regulated latest arrival time $T_{\text{arrival}}[k]$ at each station according to the timetable of the railway route.

$$0 \leqslant x[k] \leqslant T_{\text{arrival}}[k]. \tag{18}$$

The control variable is limited by the shortest possible drive time $T_{\text{drive, min}}[k]$ and the maximal drive time $T_{\text{drive, max}}[k]$ of the k-th railway section.

$$T_{\text{drive, min}}[k] \leqslant u[k] \leqslant T_{\text{drive, max}}[k]. \tag{19}$$

The shortest possible drive time is calculated according to speed limit and corresponding acceleration limit, and the longest possible drive time is defined by the timetable. Notably, the control variable, namely the drive time between two adjacent stations, is not constant but varies at each railway section.

The cost function calculates the total energy consumption for the entire railway route with multiple sections. For a driving cycle with L railway sections, the entire energy cost J is described as:

$$J = \underbrace{\sum_{k=1}^{L} E(u[k])}_{\text{energy consumption}}, \tag{20}$$

where $E(u[k])$ represents the minimal energy consumption corresponding to different drive times between two stations.

The initial state is defined as $x[0] = 0$, which means the initial state of all possible trajectories equals zero. The trajectories with non-zero initial state are assigned with invalid value, so that they will not be selected, as shown in Fig. 8. A forward iteration is applied to obtain the optimal drive time distribution. When the L-th stage is finished, a trace-back is required to get the optimal control trajectory, namely the optimal drive time of each railway section. At the end, the speed trajectories corresponding to the optimal drive time of different railway sections are connected together, with the stop time at each station added in between. The optimal speed profile for the entire railway route among multiple stations is thus obtained.

3.4. Results

For the railway route from Bremervörde to Cuxhaven with 14 stations, the minimal possible drive time is 4615 s, and the maximal allowed drive time is 6540 s. The maximal drive time is chosen to be the total drive time of the timetable. Each value between maximal and minimal drive time is possible, and the corresponding energy consumption is shown in Fig. 9. In the same manner as in

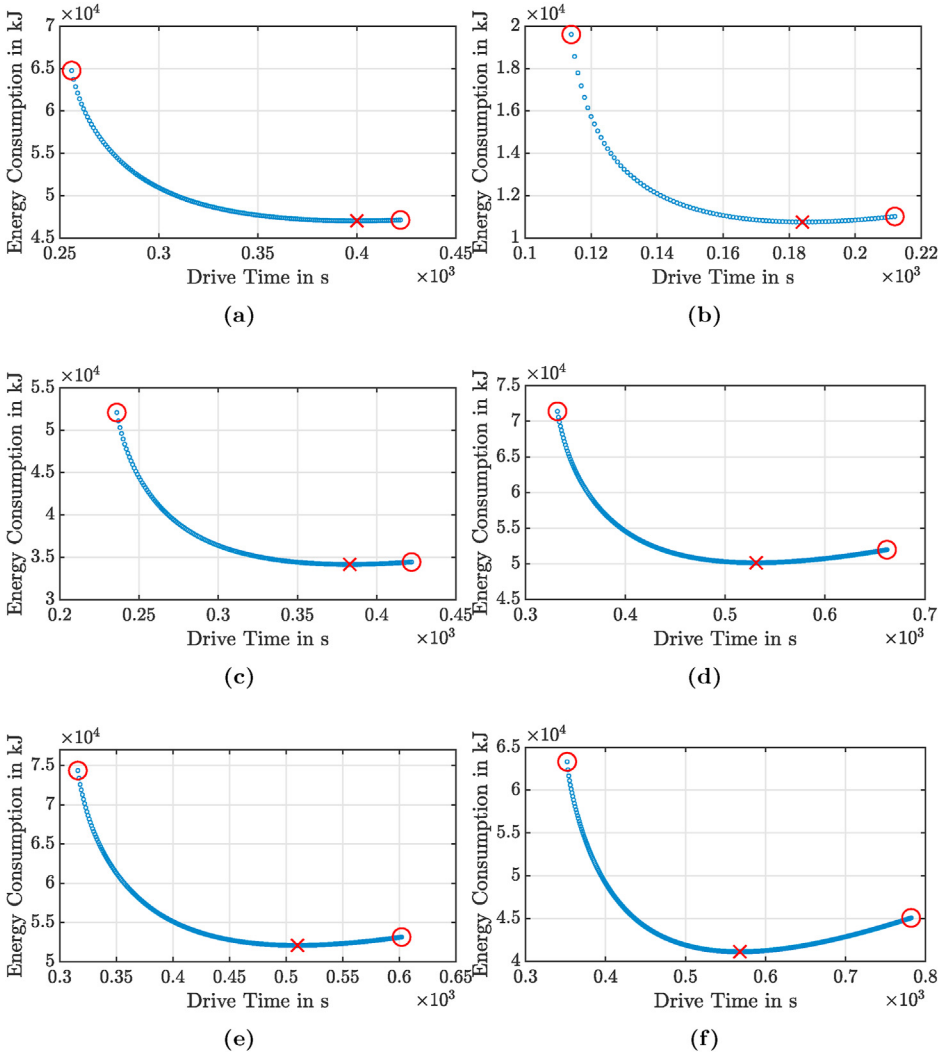

Fig. 7. Energy consumption corresponding to each drive time of several sections: (a) Section 1, (b) Section 4, (c) Section 7, (d) Section 10, (e) Section 12, (f) Section 13.

Table 5
Different drive time and the corresponding energy consumption.

Section	Shortest drive time	Longest drive time	Optimal drive time
1	256 s : 64762 kJ	422 s : 47127 kJ	400 s : 47024 kJ
2	150 s : 28272 kJ	212 s : 17032 kJ	212 s : 17032 kJ
3	181 s : 27556 kJ	242 s : 14821 kJ	242 s : 14821 kJ
4	114 s : 19611 kJ	212 s : 11018 kJ	184 s : 10757 kJ
5	149 s : 28657 kJ	182 s : 19396 kJ	182 s : 19396 kJ
6	202 s : 43444 kJ	302 s : 28252 kJ	302 s : 28252 kJ
7	236 s : 52082 kJ	422 s : 34441 kJ	383 s : 34162 kJ
8	133 s : 26497 kJ	212 s : 16795 kJ	212 s : 16795 kJ
9	146 s : 31482 kJ	242 s : 20132 kJ	235 s : 20116 kJ
10	332 s : 71402 kJ	662 s : 51966 kJ	531 s : 50130 kJ
11	207 s : 44413 kJ	332 s : 28724 kJ	332 s : 28724 kJ
12	316 s : 74360 kJ	602 s : 53138 kJ	510 s : 52072 kJ
13	352 s : 63319 kJ	782 s : 45062 kJ	568 s : 41103 kJ

Table 6
Distance deviation and calculation demands of each driving section with the optimal drive time.

Section	Real distance	Cal. distance	Difference	Cal. time	RAM memory
1	7842 m	7842.35 m	0.35 m	1h49min	61.43 GB
2	3737 m	3737.35 m	0.35 m	30min	24.47 GB
3	4987 m	4987.36 m	0.36 m	39min	34.41 GB
4	2489 m	2490.75 m	1.75 m	15min	15.01 GB
5	3710 m	3710.75 m	0.75 m	29min	24.22 GB
6	5789 m	5789.51 m	0.51 m	1h03min	41.59 GB
7	7300 m	7300.75 m	0.75 m	1h53min	55.58 GB
8	3090 m	3090.32 m	0.32 m	20min	19.22 GB
9	3668 m	3668.83 m	0.83 m	27min	23.85 GB
10	11128 m	11128.42 m	0.42 m	1h20min	49.5 GB
11	5997 m	5997.42 m	0.42 m	55min	43.42 GB
12	10757 m	10757.34 m	0.34 m	1h31min	46.96 GB
13	12133 m	12133.40 m	0.40 m	1h41min	55.66 GB

the previous part, the minimal and maximal drive time points and the optimal drive time are highlighted with circles and a cross symbol. The drive time corresponding to minimal energy consumption is 6045 s, which is about 8 min shorter than the 6540 s drive time of the timetable. Their corresponding energy consumption is listed in Table 7, with the optimal driving cycle 1.8 % less than the existing time tables. The generated optimal speed profile with a total drive time of 6045 s is presented in Fig. 10. It is worth noting that the energy curve rises slightly after the time point corresponding to the minimal energy consumption, because the energy consumed by auxiliaries increases linearly when the drive time prolongs and becomes a non-negligible part of the total energy consumption. As a result of the high discretization degree,

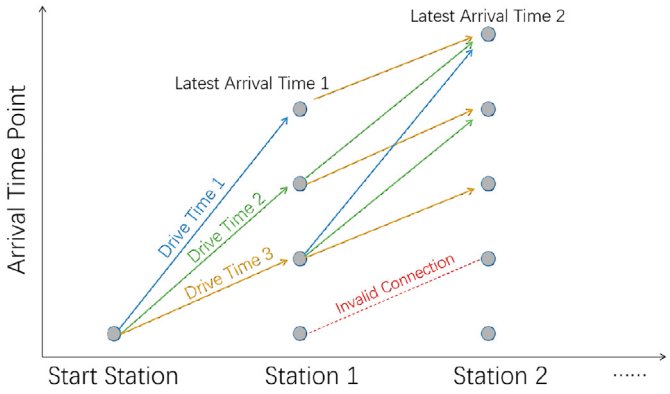

Fig. 8. Transition pattern of the state matrix.

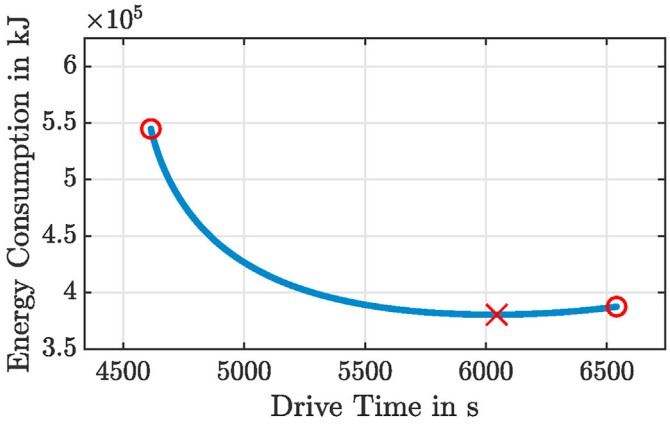

Fig. 9. Energy consumption corresponding to each total drive time.

Table 7
Results of the total running time optimization.

Shortest total running time	4615 s : 544624 kJ
Longest total running time	6540 s : 387520 kJ
Optimal total running time	6045 s : 380424 kJ
Real distance	82627 m
Calculated distance	82633.97 m
Difference in distance	6.97 m
Total calculation time	13h28 m
Utilized memory	64.31 GB

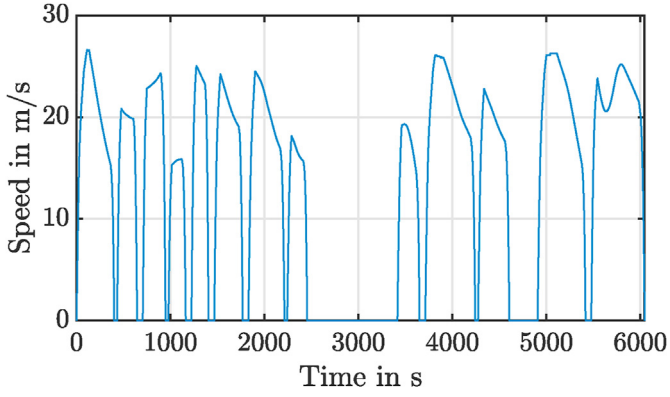

Fig. 10. Optimal speed profile for Alstom Coradia iLint route from Bremervörde to Cuxhaven.

the calculated distance's total deviation is only 6.97 m. Additionally, the total calculation time and memory utilization can be found in Table 7.

4. Rule-based power distribution strategy

When discussing the real-time applications of energy management strategies for a train, the computational load must be taken into account. The rule-based strategies are suitable for the online-application and easy to implement due to the low computational burden and robustness. Those advantages allow them to be broadly applied in commercial hybrid vehicles. In this section, a rule-based power distribution strategy is introduced, and the main drawbacks of the rule-based strategies such as restricted optimality and adaptivity are avoided by developing a quantitative formula that emphasizes the specific consumption curve's convexity.

4.1. Principals of the rule-based power distribution method

In the previous section, the fuel cell system's specific consumption curve is displayed. According to its convexity, the fuel efficiency of concentrating the fuel cell power near its global average value is better than distributing the operating points. Additionally, the charge-sustaining condition of the battery is to be fulfilled, which means the total load energy should be provided by the fuel cells as follows:

$$\int_{t_0}^{T} P_{\mathrm{fc}}(\tau)\,\mathrm{d}\tau = \int_{t_0}^{T} \left(P_{\mathrm{load}}(\tau) + P_{\mathrm{bat,\,loss}}(\tau)\right)\,\mathrm{d}\tau, \tag{21}$$

where T is the total drive time, P_{fc} the fuel cell output power, P_{load} the load power and $P_{\mathrm{bat,\,loss}}$ the battery loss power. Besides, the principle of load follower is also implemented in the strategy. When the SoC of battery lies in a middle range, the fuel cell output power equals the global mean value of the load power. When the SoC is low, the fuel cell output power will be adjusted to be $(1+a)$ of the average value. On the contrary, the fuel cell output power is decreased by a factor b when the SoC is high. In this contribution, the factor a and b are set to be 0.33 and 0.4, respectively. Its mechanism is displayed in Fig. 11. The estimation method of the global mean load power and other details of the rule-based strategy can be found in Ref. [39]. It is worth noting that the estimated average load power is updated when the rail vehicles leave the stations in between. Besides, the effectiveness of this strategy is validated by experiments on a testbench with hardware-in-the-loop [41].

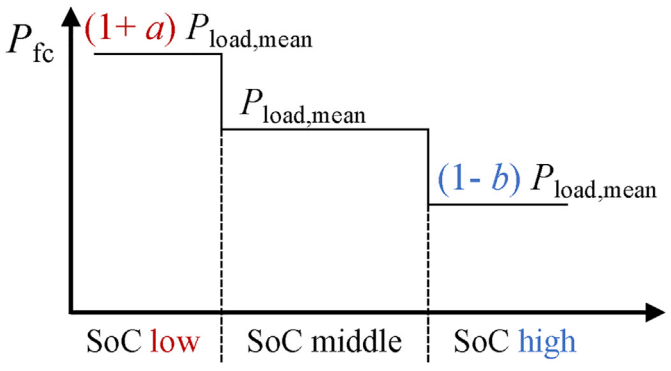

Fig. 11. Mechanism of the rule-based strategy.

4.2. Simulation results

Analog to the last section, the iLint railway route with 14 stops is chosen as the test route, having a total distance of 82.6 km. The optimal speed trajectory generated by dynamic programming is the input of the online simulation model.

The power distribution of the simulation results under the rule-based strategy is displayed in Fig. 12. The fuel cell output power is controlled to equal the mean value of the load power history. The rest of the load power, which has high fluctuation, is supplied by the battery. Fig. 13 shows the SoC trajectories as well as the fuel cell system power. The end status of SoC lies at 0.5001, which is almost identical with the initial value 0.5000. The simulated hydrogen consumption is 17676 g for the whole train on the given route in summer.

To evaluate the rule-based power distribution method, its result is compared with the result of a PMP-based offline strategy [41]. Hereinafter, the PMP-based offline strategy is referred to as the reference strategy. As a global strategy, the reference strategy requires information about the entire driving cycle in advance, and can therefore find the global optimum of a given problem. Fig. 14 shows the fuel cell system output power and the SoC trajectories of these two strategies.

The hydrogen consumption in summer calculated by the reference strategy comprises 17656 g, which is 20 g less than the result of the rule-based strategy. Thus, the rule-based strategy is proven to achieve excellent fuel economy with only 0.11 % more consumption compared to the reference strategy, in terms of Alstom iLint route in summer. Detailed results of both strategies are listed in Table 8. Besides, the fuel cell power under the rule-based strategy remains constant between every two stations, which also helps to prolong the lifetime of the fuel cell system.

5. Co-optimization of driving cycles and energy management strategies

As introduced in section 3, the speed profile of a given railway route is generated based on the terrain information, the timetable, and the power limits of energy sources, without considering the energy management strategy. Then in section 4, the established velocity profile is taken as prior knowledge for determining power distribution between fuel cells and batteries. Notably, the results from the energy management strategy can also contribute to improving the accuracy of the speed profile by serving as inputs for dynamic programming. Thereby, in the second implementation of dynamic programming, the current limits of batteries are considered instead of the power limits, which improve the accuracy of the renewed speed profile. Therefore, a co-optimization of speed profile and energy management helps to take advantage of fuel cell hybrid configuration fully. In this part, the sequential optimization approach is applied to implement the co-optimization.

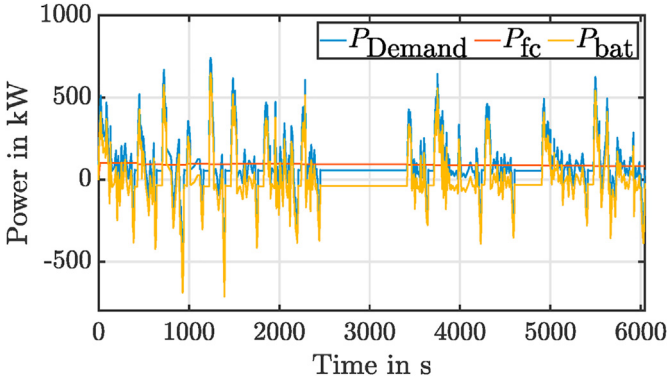

Fig. 12. Power distribution results of online simulation under the rule-based strategy.

5.1. Introduction of the sequential optimization approaches

Sequential optimization approaches are adopted in this work to maintain the computational load of co-optimization acceptable. In the speed profile optimization, speed and location are defined as two state variables to formulate the optimal control problem. In energy management strategy optimization, the SoC is chosen as the state variable in most literature relating to dynamic programming. Thus, if the co-optimization is implemented using parallel approaches, the number of state variables increases from two to three. A huge amount of calculation is inevitable considering the discretization degree in velocity, position, SoC, and time.

With sequential optimization approaches, the first version of the speed profile is determined without information on power distribution. Then, the generated speed profile serves as an input in determining power distribution between fuel cells and batteries. With the rule-based strategy's help, the trajectory of fuel cell power and SoC of batteries for each railway section is defined. The SoC initial value in each section and the fuel cell power trajectory for the same section are used as inputs of the dynamic programming algorithm so that the renewed version of the speed profile is generated with the influence of power distribution considered. The speed profile with accuracy improved can be sent back to the rule-based strategy to optimize power distribution. The iteration can be repeated multiple times to refining the result if necessary. Thus, the computational time of calculating each iteration stays at a similar level as before, with an affordable increase of time caused by additional calculation.

5.2. Implementation of the co-optimization mechanism

When generating driving cycles with dynamic programming, the velocity profile is firstly generated between every two stations. According to the rule-based strategy, the fuel cell system power is updated at each stop. Therefore, the fuel cell system power resulted from energy management can work as an input to the dynamic programming algorithm.

As the fuel cell power of each section is given, the battery power can be obtained:

$$P_{\mathrm{bat}}[k](x_1[k],u[k]) = P[k](x_1[k],u[k]) - P_{\mathrm{fc}}[k], \tag{22}$$

where $P[k](x_1[k],u[k])$ is the load power, $P_{\mathrm{fc}}[k]$ relates to the fuel cell system power of the k-th stage and $P_{\mathrm{bat}}[k](x_1[k], u[k])$ is the battery power of the k-th stage. After the battery power is obtained, it can be transformed into a variation in SoC with the following equations.

If $P_{\mathrm{bat}}[k] \geqslant 0$:

$$\Delta SoC[k](x_1[k],x_2[k],u[k]) = \frac{P_{\mathrm{bat}}[k](x_1[k],u[k])\cdot\Delta t}{Q_{\mathrm{bat}}\cdot V_{\mathrm{oc}}(SoC[k-1])}\cdot\frac{1}{\eta_{\mathrm{discharge}}}, \tag{23}$$

if $P_{\mathrm{bat}}[k] < 0$:

$$\Delta SoC[k](x_1[k],x_2[k],u[k]) = \frac{P_{\mathrm{bat}}[k](x_1[k],u[k])\cdot\Delta t}{Q_{\mathrm{bat}}\cdot V_{\mathrm{oc}}(SoC[k-1])}\cdot\eta_{\mathrm{charge}}, \tag{24}$$

where $\Delta SoC[k](x_1[k], x_2[k], u[k])$ is the SoC variation, Q_{bat} describes the battery capacity, V_{oc} is the open circuit voltage, $\eta_{\mathrm{discharge}}$ the discharge efficiency and η_{charge} refers to the charge efficiency of the batteries. The values of $\eta_{\mathrm{discharge}}$ and η_{charge} are calculated with the

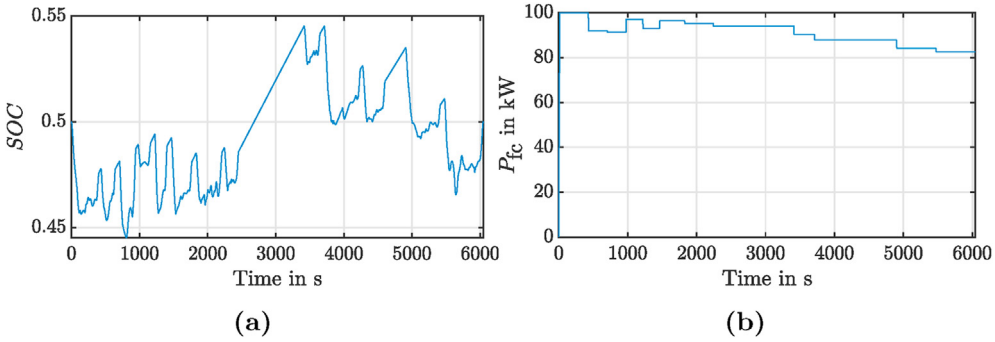

Fig. 13. SoC and fuel cell system power trajectories after online simulation. (a) SoC, (b) Fuel cell system power.

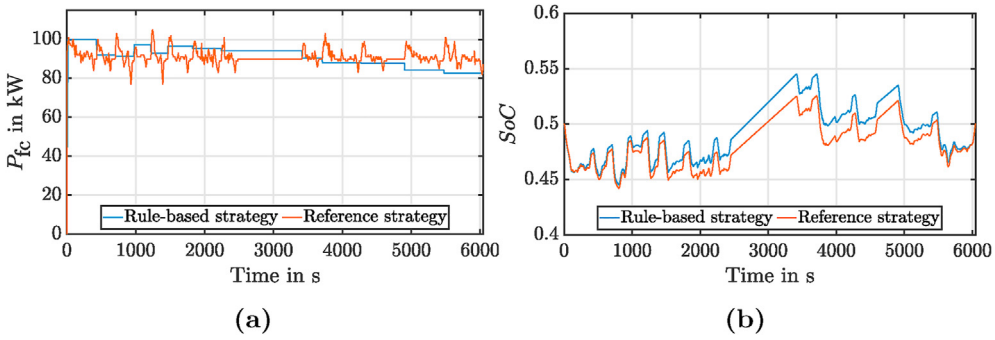

Fig. 14. Comparison between the rule-based strategy and the PMP reference strategy regarding: (a) Fuel cell system power trajectories, (b) SoC trajectories.

Table 8
Comparison between the rule-based strategy and the reference strategy.

Item	Rule-based strategy	Reference strategy
SoC_{end}	0.5001	0.5001
Averaged fuel cell power	91.0526 kW	91.0054 kW
Total drive time	6045 s	6045 s
Hydrogen consumption	17676 g	17656 g
Consumption pro km (full train)	213.93 g	213.68 g
Hydrogen increase compared to reference	0.11 %	/

averaged battery voltage and the averaged open circuit voltage during the online simulation. It is worth mentioning that, when calculating ΔSoC of the k-th stage, the corresponding value of V_{oc} is interpolated with the SoC of the (k-1)-th stage.

Then, the SoC matrix of the current stage corresponding to all controls is determined. In the first time stage, the adjustment of the SoC matrix is formulated as follows:

$$SoC[1](x_1[1], x_2[1], u[1]) = SoC_{\text{init, section}} + \Delta SoC[1](x_1[1], x_2[1], u[1]), \quad (25)$$

where $SoC_{\text{init, section}}$ is the SoC at the beginning of the section. In other time stages, the adjustment of the SoC matrix is:

$$SoC[k](x_1[k], x_2[k], u[k]) = SoC[k-1](x_1[k-1], x_2[k-1], u[k-1]) + \Delta SoC[k](x_1[k], x_2[k], u[k]). \quad (26)$$

With the SoC matrix corresponding to all the inputs of k-th stage, the matrix of open circuit voltage $V_{oc}[k](SoC[k])$ and the resistance $R_0[k](SoC[k])$ are determined with interpolation. With these values, the matrix of the battery current $I_{bat}[k](x_1[k], x_2[k], u[k])$ is calculated with the following equation:

$$I_{bat}[k](x_1[k], x_2[k], u[k]) = \frac{V_{oc}[k](SoC[k])}{2 \cdot R_0[k](SoC[k])} - \frac{\sqrt{V_{oc}[k](SoC[k])^2 - 4 \cdot P_{bat}[k] \cdot R_0[k](SoC[k])}}{2 \cdot R_0[k](SoC[k])}. \quad (27)$$

If a value in matrix $I_{bat}[k]$ is greater than the given limit of battery current $I_{bat,\ max}$ or less than $I_{bat,\ min}$, the transition cost of the

Table 9
Results of the total running time after co-optimization.

Shortest total running time	4514 s : 575856 kJ
Longest total running time	6540 s : 387483 kJ
Optimal total running time	6045 s : 380385 kJ
Real distance	82627 m
Calculated distance	82634.04 m
Difference in distance	7.04 m
Total calculation time	31h
Utilized memory	86.18 GB

corresponding control is allocated with an invalid value, to exclude this control in the selection of optimal control trajectory. The detailed workflow is displayed in Fig. 15 and summarized as follows:

- Step 1: the cost-to-go values of all states in Eq. (11) are initialized at the start time.
- Step 2: the SoC matrix $SoC[0]$ is initialized with $SoC_{\text{init, section}}$ and the initial open circuit voltage $V_{\text{oc, init}}(SoC[0])$ is determined with interpolation.
- Step 3: the states of the $(k-1)$-th stage $x_1[k-1]$ and $x_2[k-1]$ under different $u[k]$ are calculated with Eq. (6) and Eq. (7), respectively.
- Step 4: the matrix of transition cost $P[k](x_1[k], u[k])$ and its corresponding battery power $P_{\text{bat}}[k](x_1[k], u[k])$ is calculated with Eq. (22).
- Step 5: $\Delta SoC[k](x_1[k], x_2[k], u[k])$ is determined with Eq. (23) or Eq. (24) and $SoC[k](x_1[k], x_2[k], u[k])$ is updated.
- Step 6: $V_{\text{oc}}[k](SoC[k])$ and $R_{\text{bat}}[k](SoC[k])$ are determined with interpolation, and $I_{\text{bat}}[k](x_1[k], u[k])$ is calculated with Eq. (27).
- Step 7: invalid values of $I_{\text{bat}}[k](x_1[k], u[k])$ are detected and the corresponding transition costs are neglected.
- Step 8: the cost-to-go matrix in the $k-1$-th time stage is calculated by interpolation.
- Step 9: the rest of the transition cost $P[k](x_1[k], u[k])$ is added to the cost-to-go matrix of $(k-1)$-th stage.
- Step 10: the optimal control $u[k]$ is determined by applying the Bellman's principle of optimality.
- Step 11: the cost-to-go matrix in the k-th time stage and $SoC[k](x_1[k], x_2[k], u[k])$ are updated.
- Step 12: if the final time stage N is not reached, back to step 3.

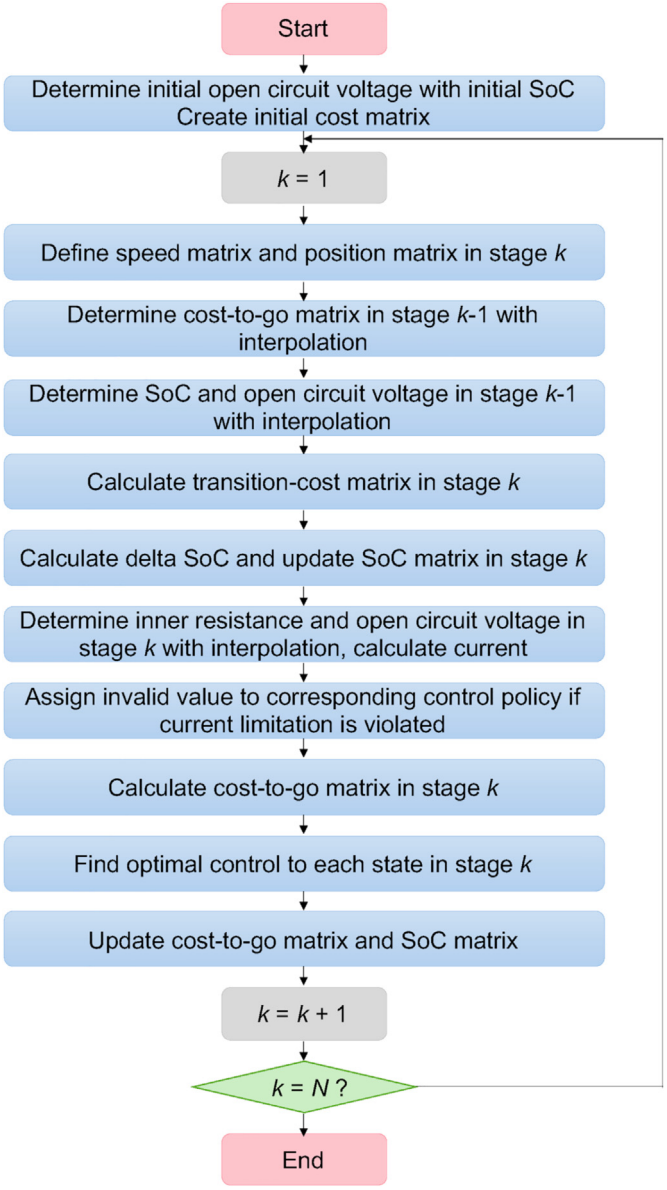

Fig. 15. Speed trajectory optimization between two stations with fuel cell power and battery current limit considered.

As a result, a more accurate speed profile is generated, in which the trajectory of fuel cell power and the battery current limits are considered. Then, the power distribution can be optimized in the rule-based strategy with the updated driving cycle. Through this method, the mutual influence of the speed profile and energy management is fully considered.

5.3. Results

In the same manner as in previous sections, the railway route with 14 stops from Bremervörde to Cuxhaven is chosen to generate the speed profile. The total distance is 82.6 km. The original speed profile is determined based on the terrain information, the timetable, and the power limit of both the fuel cell and the battery. Fig. 16 displays the generated velocity trajectory under a total drive time of 4615 s, which is also the shortest possible drive time. Taking this speed profile as input, the power distribution is then determined in the rule-based strategy. The resulted trajectories of SoC, power demand, and fuel cell system power, as well as the power distribution, are shown in Fig. 17.

Since the trajectory of fuel cell power is determined, and the SoC of batteries upon departure at each train station is available, they will be used in the dynamic programming to improve the speed profiles' optimization. In the next step, the battery current limits are considered instead of the battery system's power limit. The second execution of dynamic programming then generates the optimized speed profile considering the influence of energy management. Fig. 18 presents the Pareto front between energy consumption and drive time before and after co-optimization.

Notably, the speed profile algorithm after co-optimization shows better performance when the drive time is shorter. The

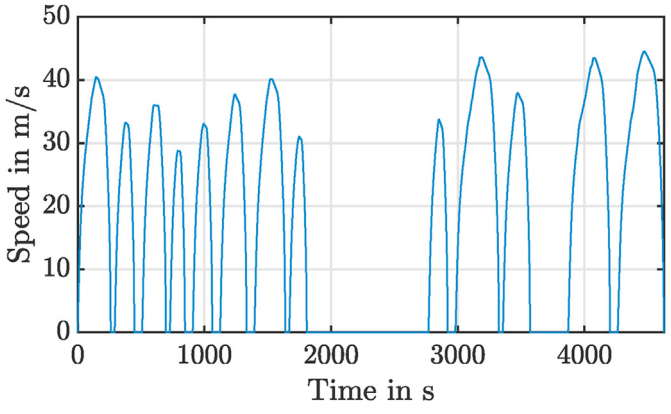

Fig. 16. Original speed profile for a drive time of 4615 s without considering the influence of EMS.

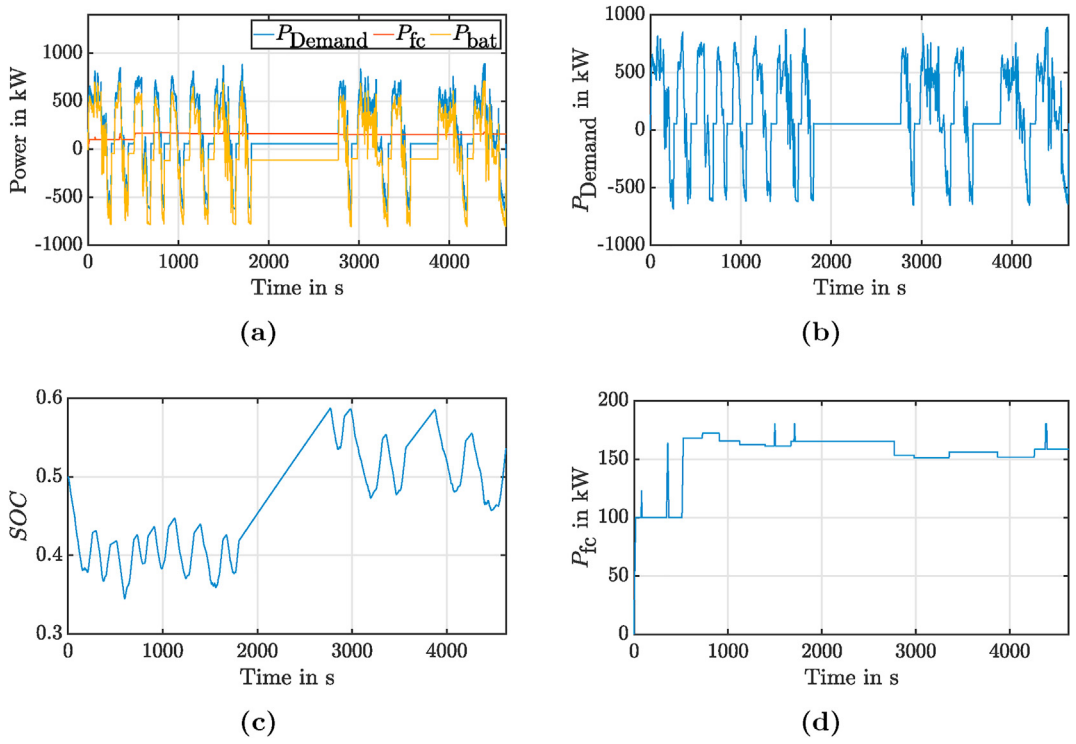

Fig. 17. Online simulation results based on the original speed profile for the minimal drive time of 4615 s: (a) Power distribution, (b) Load power demand, (c) SoC, (d) Fuel cell system power.

lowest point of the Pareto curves indicates minimal energy consumption. Obviously, the minimal energy consumption shows no remarkable difference before and after co-optimization, as the two curves stay quite close with each other for the drive time longer than 5000 s. The corresponding drive time of minimal energy consumption also lies in this area. The drive time corresponding to minimal energy consumption is 6045 s, and it is highlighted with a red cross in the figure. The corresponding energy consumption is listed in Table 9. Therefore, the generated optimal speed profiles corresponding to minimal energy consumption are also almost identical before and after co-optimization, shown in Fig. 19. The speed profile after co-optimization is represented as a red curve. It has almost the same trajectory as the speed profile before co-optimization, which is represented as a blue curve so that the red

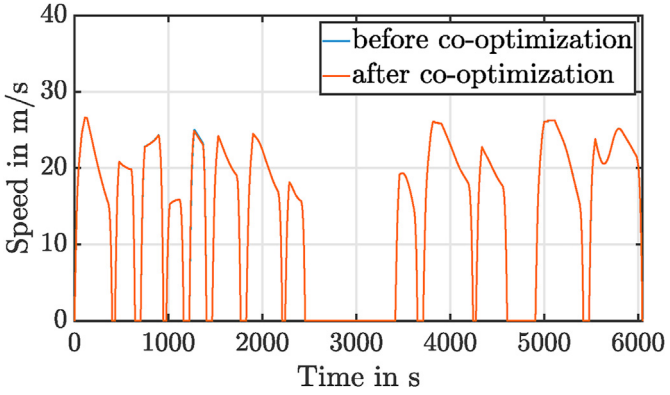

Fig. 19. Speed profile before and after co-optimization for a drive time of 6045 s.

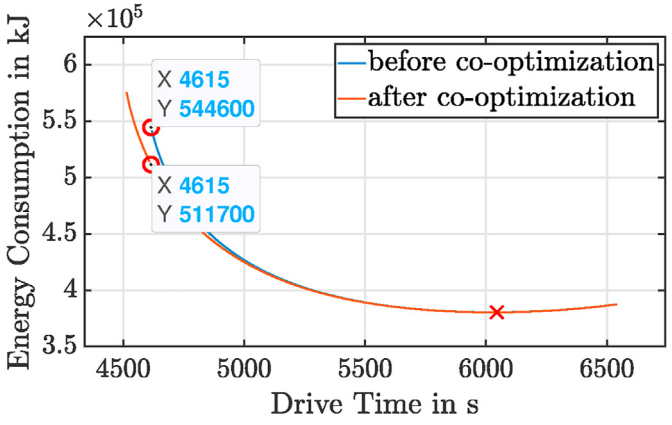

Fig. 18. Energy consumption corresponding to drive time before and after co-optimization.

curve completely covers the blue one. The deviation of calculation in the distance and the computational demands are listed in Table.9. The total calculation time and memory utilization have increased to 31 h and 86.18 GB, respectively, which is much higher than before the co-optimization. Because in each step of the second execution of dynamic programming, several additional matrices such as the SoC and the battery current need to be calculated, which have considerable computational demands due to their large size.

However, there is an obvious improve on the consumption when a short drive time is required. The earliest arrival time before co-optimization lies at 4615 s. Taking a total drive time of 4615 s for instance, the train consumes 511700 kJ energy after co-optimization, which is 32900 kJ less compared with 544600 kJ before co-optimization. The energy is saved by 6.04 % in this case. Both points for energy consumption corresponding to drive time of

Table 10
Earliest arrival time before and after co-optimization.

Item	Before co-optimization	After co-optimization
Earliest arrival time	4615 s	4514 s
Time saving in %	2.19 %	/

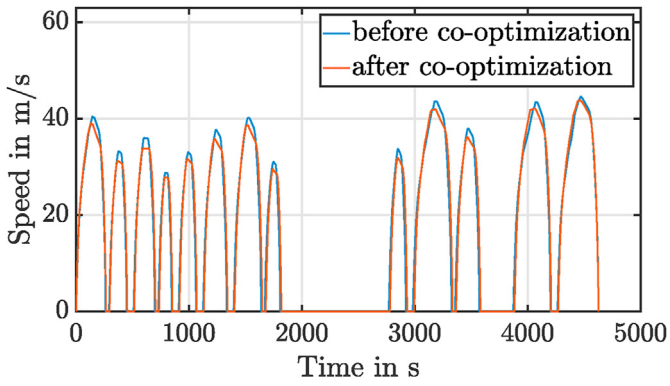

Fig. 20. Speed profile before and after co-optimization for a drive time of 4615 s.

4615 s are marked with red circles in Fig. 18. Besides, the co-optimization helps to reach a shorter drive time for the given route. The earliest possible arrival time lies at 4514 s after co-optimization, which is 101 s shorter compared with 4615 s before co-optimization. The shortest possible drive time decreases by 2.19 % in this case, shown in Table 10.

A comparison of speed profile before and after co-optimization for a total drive time of 4615 s is presented in Fig. 20. The new speed profile considers the influence of the power distribution. Therefore, it is able to take full advantage of the hybrid power train configuration. Taking the new speed profile as input, a better power distribution can be determined by the rule-based strategy. A comparison of the SoC and the fuel cell system power before and after co-optimization is presented in Fig. 21. After co-optimization, the SoC trajectory shows less fluctuation and the fuel cell system power stays stable with a lower average power. It is worth noting that in the fuel cell output power trajectories, some peak values exist because the low SoC mode is activated and the fuel cell power is increased by the factor a than the mean load power. The simulation results before and after co-optimization are summarized in Table 11. 25142 g hydrogen is consumed for Alstom iLint route in summer, with a total drive time of 4615 s. Compared with the results before co-optimization, 3.80 % saving on hydrogen consumption is achieved.

Table 11
Simulation results before and after co-optimization for a drive time of 4615 s.

Item	Before co-optimization	After co-optimization
SoC_{end}	0.5360	0.5222
Averaged fuel cell power	153.75 kW	149.62 kW
Simulation time	4615 s	4615 s
Hydrogen consumption	26136 g	25142 g
Consumption pro km	316.31 g	304.28 g
Consumption decrease	/	3.80 %

6. Conclusions

In this work, the co-optimization of the total running time, timetables, driving strategies, and energy management strategies of the hydrogen-powered hybrid train is introduced. Firstly, a two-dimensional forward dynamic programming algorithm is utilized to generate the speed profile between two railway stations considering the continuous varying speed limits and gradients. The computational efficiency is improved through the parallelization of the algorithm by interpolative estimation of the cost-to-go values. Besides, with a tricky initialization of the cost matrix, the boundary problem is solved, forcing the initial values of the state variables to be zero. With the aid of the Pareto solutions, the optimal drive times that minimize the energy consumption can be found. Next, the whole journey's total drive time, and the optimal time table, which describes the optimal drive time distribution between the railway sections, are determined by the second dynamic programming execution. For a driving cycle of 82.6 km, the calculated distance deviation due to discretization is 6.97 m and the total calculation time is 13.5 h. The optimal running time of 6045 s with minimal energy consumption is determined, which is about 8 min less than the existing timetable and consumes 1.8 % less energy.

As for the energy management strategy, a rule-based online strategy is used. The rule-based strategy utilizes the specific consumption curve's convexity, which combines the advantages of optimality, adaptivity, stable operation of fuel cell systems, and scalability. Its result, which is the power distribution between the battery and the fuel cell, is used to improve speed profile accuracy. Thereby, a sequential optimization is introduced to realize the decoupling, which maintains the number of state variables at two and reduces the computational cost. After the co-optimization, a shorter drive time to a given route can be found and the energy consumption is obviously reduced if a short driving time is required. In terms of the *Alstom iLint1* route, no remarkable difference is presented before and after co-optimization for the drive time of 6045 s corresponding minimal energy consumption. However, if a short drive time of 4615 s is expected, the energy consumption is saved by 6.04 % after co-optimization compared to the value before co-optimization. Meanwhile, with the optimized

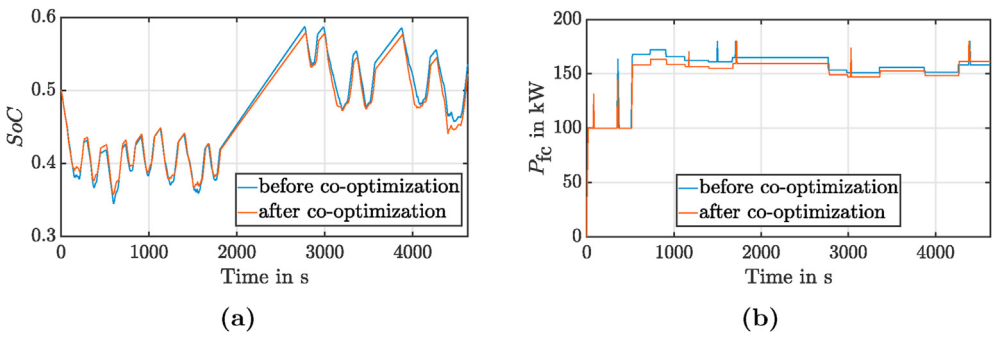

Fig. 21. EMS results before and after co-optimization for a drive time of 4615 s: (a) SoC, (b) fuel cell system power.

speed profile, the energy management strategy's hydrogen consumption decreases by 3.8 %.

CRediT authorship contribution statement

Hujun Peng: Conceptualization, Methodology, Formal analysis, Validation, Writing – original draft. **Yuejie Chen:** Data curation, Writing – original draft. **Zhu Chen:** Software, Data curation, Writing – original draft. **Jianxiang Li:** Software, Formal analysis. **Kai Deng:** Writing – review & editing. **Andreas Thul:** Writing – review & editing, Project administration. **Lars Löwenstein:** Resources, Writing – review & editing. **Kay Hameyer:** Supervision, Funding acquisition, Writing – review & editing.

Declaration of competing interest

The authors declare that they have no known competing financial interests or personal relationships that could have appeared to influence the work reported in this paper.

References

[1] Tracking transport 2020, https://www.iea.org/reports/tracking-transport-2020, accessed October 19, 2020.
[2] A european strategy for low-emission mobility, https://ec.europa.eu/clima/policies/transport_en, accessed October 19, 2020.
[3] Tracking transport 2020/rail, https://www.iea.org/reports/tracking-transport-2020/rail#abstract, accessed October 19, 2020.
[4] Daten & fakten zur schieneninfrastruktur, https://www.allianz-proschiene.de/themen/infrastruktur/daten-fakten/, accessedOctober 19, 2020.
[5] H. Jürgen, Auf dem weg zur null-emmision, eisenbahn-magazin.
[6] China has world's first hydrogen tram, https://www.gasworld.com/china-has-worlds-first-hydrogen-tram-/2013703.article, accessed October 28, 2020.
[7] Stadler to deliver hydrogen-powered train to sbcta, https://www.railway-technology.com/news/stadler-deliver-hydrogenpowered-train-sbcta/, accessed October 28, 2020.
[8] Yang S, Wu J, Yang X, Sun H, Gao Z. Energy-efficient timetable and speed profile optimization with multi-phase speed limits: theoretical analysis and application. Appl Math Model 2018;56:32–50.
[9] Yang X, Li X, Ning B, Tang T. A survey on energy-efficient train operation for urban rail transit. IEEE Trans Intell Transport Syst 2016;17(1):2–13. https://doi.org/10.1109/TITS.2015.2447507.
[10] Scheepmaker GM, Goverde RMP, Kroon LG. Review of energy-efficient train control and timetabling. Eur J Oper Res 2017;257(2):355–76.
[11] Khmelnitsky E. On an optimal control problem of train operation. IEEE Trans Automat Contr 2000;45(7):1257–66. https://doi.org/10.1109/9.867018.
[12] Albrecht A, Howlett P, Pudney P, Vu X, Zhou P. The key principles of optimal train control—part 1: formulation of the model, strategies of optimal type, evolutionary lines, location of optimal switching points. Transp Res Part B Methodol 2016;94(1):482–508. https://doi.org/10.1016/j.trb.2015.07.023.
[13] Albrecht A, Howlett P, Pudney P, Vu X, Zhou P. The key principles of optimal train control—part 2: existence of an optimal strategy, the local energy minimization principle, uniqueness, computational techniques. Transp Res Part B Methodol 2016;94(2):509–38. https://doi.org/10.1016/j.trb.2015.07.024.
[14] Liu R, Golovitcher IM. Energy-efficient operation of rail vehicles. Transport Res Pol Pract 2003;37(10):917–32. https://doi.org/10.1016/j.tra.2003.07.001.
[15] Ye H, Liu R. Nonlinear programming methods based on closed-form expressions for optimal train control. Transport Res C Emerg Technol 2017;82:102–23.
[16] Howlett PG, Pudney PJ, Vu X. Local energy minimization in optimal train control. Automatica 2009;45(11):2692–8. https://doi.org/10.1016/j.automatica.2009.07.028.
[17] Goverde RM, Scheepmaker GM, Wang P. Pseudospectral optimal train control. Eur. J. Oper. Res. 2021 Jul;1292(1):353–75. https://doi.org/10.1016/j.ejor.2020.10.018.
[18] Wang P, Goverde RM. Multiple-phase train trajectory optimization with signalling and operational constraints. Transport Res C Emerg Technol 2016;69(3):255–75. https://doi.org/10.1016/j.trc.2016.06.008.
[19] Scheepmaker GM, Goverde RMP. Energy-efficient train control using nonlinear bounded regenerative braking. Transport Res C Emerg Technol 2020;121:102852.
[20] Lu S, Wang MQ, Weston P, Chen S, Yang J. Partial train speed trajectory optimization using mixed-integer linear programming. IEEE Trans Intell Transport Syst 2016;17(10):2911–20.
[21] Wang Y, de Schutter B, van den Boom TJ, Ning B. Optimal trajectory planning for trains – a pseudospectral method and a mixed integer linear programming approach. Transport Res C Emerg Technol 2013;29:97–114. https://doi.org/10.1016/j.trc.2013.01.007.
[22] Li X, Lo HK. An energy-efficient scheduling and speed control approach for metro rail operations. Transp Res Part B Methodol 2014;64:73–89.
[23] Lu S, Hillmansen S, Ho TK, Roberts C. Single-train trajectory optimization. IEEE Trans Intell Transport Syst 2013;14(2):743–50. https://doi.org/10.1109/TITS.2012.2234118.
[24] H. Ko, T. Koseki, M. Miyatake, Application of dynamic programming to the optimization of the running profile of a train, WIT Trans Built Environ 74. doi: 10.2495/CR040111.
[25] Miyatake M, Ko H. Optimization of train speed profile for minimum energy consumption. IEEJ Trans Electr Electron Eng 2010;5(3):263–9.
[26] Haahr JT, Pisinger D, Sabbaghian M. A dynamic programming approach for optimizing train speed profiles with speed restrictions and passage points. Transp Res Part B Methodol 2017;99(10):167–82. https://doi.org/10.1016/j.trb.2016.12.016.
[27] B R, et al. The theory of dynamic programming. Bull Am Math Soc 1954;60(6):503–15.
[28] Xu P, Feng G, Cui D, Dai X, Zhang Q, Chen F. Timetable mapping model and dynamic programming approach for high-speed railway rescheduling. In: 2020 39th Chinese control conference (CCC). IEEE; 2020. p. 1739–44.
[29] Albrecht T, Oettich S. A new integrated approach to dynamic schedule synchronization and energy-saging train control. Southampton and Boston: WIT Press; 2002.
[30] Scheepmaker GM, Goverde RMP. The interplay between energy-efficient train control and scheduled running time supplements. J. Rail.Transport. Plann.-Manag. 2015;5(4):225–39.
[31] Su S, Li X, Tang T, Gao Z. A subway train timetable optimization approach based on energy-efficient operation strategy. IEEE Trans Intell Transport Syst 2013;14(2):883–93. https://doi.org/10.1109/tits.2013.2244885.
[32] Su S, Wang X, Cao Y, Yin J. An energy-efficient train operation approach by integrating the metro timetabling and eco-driving. IEEE Trans Intell Transport Syst 2019;21(10):4252–68.
[33] Wang P, Goverde RMP. Multi-train trajectory optimization for energy-efficient timetabling. Eur J Oper Res 2019;272(2):621–35.
[34] Scheepmaker GM, Pudney PJ, Albrecht AR, Goverde RMP, Howlett PG. Optimal running time supplement distribution in train schedules for energy-efficient train control. J. Rail.Transport. Plann.Manag. 2020;14:100180.
[35] Sulaiman N, Hannan M, Mohamed A, Ker PJ, Majlan E, Daud WW. Optimization of energy management system for fuel-cell hybrid electric vehicles: issues and recommendations. Appl Energy 2018;228:2061–79.
[36] Wang Y, Wang L, Li M, Chen Z. A review of key issues for control and management in battery and ultra-capacitor hybrid energy storage systems. eTransportation 2020;4:100064. https://doi.org/10.1016/j.etran.2020.100064. https://www.sciencedirect.com/science/article/pii/S2590116820300217.
[37] Wang Y, Sun Z, Li X, Yang X, Chen Z. A comparative study of power allocation strategies used in fuel cell and ultracapacitor hybrid systems. Energy 2019;189:116142. https://doi.org/10.1016/j.energy.2019.116142. https://www.sciencedirect.com/science/article/pii/S0360544219318377.
[38] Wang Y, Li X, Wang L, Sun Z. Multiple-grained velocity prediction and energy management strategy for hybrid propulsion systems. J. Energy Storage 2019;26:100950. https://doi.org/10.1016/j.est.2019.100950. https://www.sciencedirect.com/science/article/pii/S2352152X19309405.
[39] Peng H, Li J, Thul A, Deng K, Ünlübayir C, Löwenstein L, Hameyer K. A scalable, causal, adaptive rule-based energy management for fuel cell hybrid railway vehicles learned from results of dynamic programming. eTransportation; 2020. p. 100057.
[40] Peng H, Li J, Löwenstein L, Hameyer K. A scalable, causal, adaptive energy management strategy based on optimal control theory for a fuel cell hybrid railway vehicle. Appl Energy 2020;267:114987.
[41] H. Peng, Z. Chen, J. Li, K. Deng, S. Dirkes, J. Gottschalk, C. Ünlübayir, A. Thul, L. Löwenstein, S. Pischinger, et al., Offline optimal energy management strategies considering high dynamics in batteries and constraints on fuel cell system power rate: from analytical derivation to validation on test bench, Appl Energy 282 116152.
[42] Peng H, Cao H, Dirkes S, Chen Z, Deng K, Gottschalk J, Ünlübayir C, Thul A, Löwenstein L, Sauer DU, Pischinger S, Hameyer K. Validation of robustness and fuel efficiency of a universal model-based energy management strategy for fuel cell hybrid trains: from analytical derivation via simulation to measurement on test bench. Energy Convers Manag 2021;229:113734. https://doi.org/10.1016/j.enconman.2020.113734.